Scripta Materialia 154 (2018) 159–162

Contents lists available at ScienceDirect

Scripta Materialia

journal homepage: www.elsevier.com/locate/scriptamat

Regular article

Elemental partitioning and site-occupancy in γ/γ′ forming Co-Ti-Mo and Co-Ti-Cr alloys

Hye Ji Im [a], Surendra K. Makineni [b], Baptiste Gault [b], Frank Stein [b], Dierk Raabe [b], Pyuck-Pa Choi [a,*]

[a] Department of Materials Science and Engineering, Korea Advanced Institute of Science and Technology (KAIST), 291 Daehak-ro, Yuseong-gu, Daejeon 34141, Republic of Korea
[b] Max-Planck-Institut für Eisenforschung, Max-Planck-Str. 1, 40237 Düsseldorf, Germany

ARTICLE INFO

Article history:
Received 29 March 2018
Received in revised form 23 April 2018
Accepted 25 May 2018
Available online xxxx

Keywords:
Co-based superalloy
Solute partitioning
Atom probe tomography (APT)
Site occupancy

ABSTRACT

We report on the sub-nanometer scale characterization of Co-12Ti-4Mo and Co-12Ti-4Cr (at.%) model alloys. Atom probe tomography reveals that Co and Cr partition to γ, whereas Ti and Mo to γ′. Additions of Mo and Cr to the reference Co-12Ti system lead to strong increases in γ′ volume fraction by about 25% and 12%, respectively. Element-specific spatial distribution maps along the [001] direction of the $L1_2$-ordered γ′ phase reveal that both Mo and Cr preferentially replace Ti on its sublattice. The remaining excess Ti is available for formation of additional γ′, resulting in enhanced γ′ volume fractions.

The discovery of a γ/γ′ microstructure in the Co-Al-W system, i.e. cuboidal $L1_2$-ordered $Co_3(Al,W)$ precipitates formed in a disordered fcc Co matrix, similar to Ni_3Al in the Ni-Al system, has opened new pathways for developing Co-based high-temperature alloys [1–3]. These materials show remarkable properties such as high solidus and liquidus temperatures [4], positive γ/γ′ lattice misfit [5], and large processing windows for heat treatments and thermo-mechanical processing.

However, the two-phase γ/γ′ microstructure in Co-Al-W is reported to be metastable and known to form only within a narrow compositional range [2,6]. Equilibrium phases, e.g. B2-ordered CoAl and DO_{19}-ordered Co_3W [7], can lead to a significant deterioration of mechanical properties [8]. From an engineering point-of-view, Co-Al-W alloys are not favorable for jet-engine applications due to the large amount of W required for the stabilization of γ′ precipitates and the resulting high mass density [9–11]. Stabilization of γ′ without W addition has been recently demonstrated by combined alloying of Mo/Nb [12,13] and/or Mo/Ta [14] to the Co-Al system, yielding reduced mass density. However, the γ′ phase is reported to be metastable similar to $Co_3(Al,W)$ [9].

Co-Ti is reported to be the only binary Co-based system which forms thermodynamically stable γ′ (Co_3Ti) [15] and thus, Co-Ti-based alloys are promising alternatives to Co-Al-W alloys [10,16]. γ′ precipitates formed in the Co-Ti system give rise to substantial precipitation-hardening, similar to Ni-based superalloys [17,18]. The yield strength of Co_3Ti increases with increasing temperature above 200 °C and reaches a maximum between 700 and 800 °C [19,20], thus rendering Co_3Ti an appropriate reinforcement phase at elevated temperatures. However, binary Co-Ti alloys aged at 900 °C for 100 h exhibit only a low γ′ volume fraction of about 20% due to a high solubility of Ti (~10 at.%) in fcc-Co at 900 °C [21,22]. Moreover, γ′ precipitates are prone to coarsening when exposed to high temperatures due to a γ/γ′ lattice misfit ranging from 0.75 to 1.36% [10]. In order to overcome these drawbacks, systematic studies of the effects of alloying elements on the microstructure and properties of Co-Ti-based alloys are needed. Here, we report on the effect of Mo and Cr addition to a reference Co-Ti binary alloy with the aim of increasing the γ′ volume fraction and solvus temperature and optimizing the γ/γ′ lattice misfit. We provide quantitative data on elemental partitioning, elucidate the γ′ site-occupancy behavior of the solutes by means of atom probe tomography (APT) and discuss the observed microstructures based on the APT data.

Co-12Ti, Co-12Ti-4Mo, and Co-12Ti-4Cr (in at.%) alloys were cast and re-melted at least five times using the vacuum arc re-melting (VAR) process. The as-cast alloys were homogenized between 1150 and 1160 °C for 120 h and aged at 800 °C for 24 h. For all the heat treatments, the alloys were encapsulated in quartz tubes back-filled with Ar gas. The microstructures of the aged samples were characterized by backscatter electron (BSE) imaging in a scanning electron microscope (SEM) (Zeiss Merlin). Lattice misfit values of aged samples were measured by X-ray diffraction (XRD) (RIGAKU SmartLab) using CuKα1 radiation. Detailed scans of {111} Bragg reflections were performed in the angular range from 42 to 45° at a step size of 0.02 or 0.01 and scan rate of 0.3°/min or 0.1°/min. The {111}-reflections were fitted with two Pseudo-Voigt functions and lattice parameters of γ and γ′ were obtained after deconvolution of the overlapped functions. Phase transition temperatures of aged samples were determined by differential scanning calorimetry (DSC) (NETZSCH DSC 404C). DSC measurements were

* Corresponding author.
E-mail address: p.choi@kaist.ac.kr (P.-P. Choi).

https://doi.org/10.1016/j.scriptamat.2018.05.041
1359-6462/

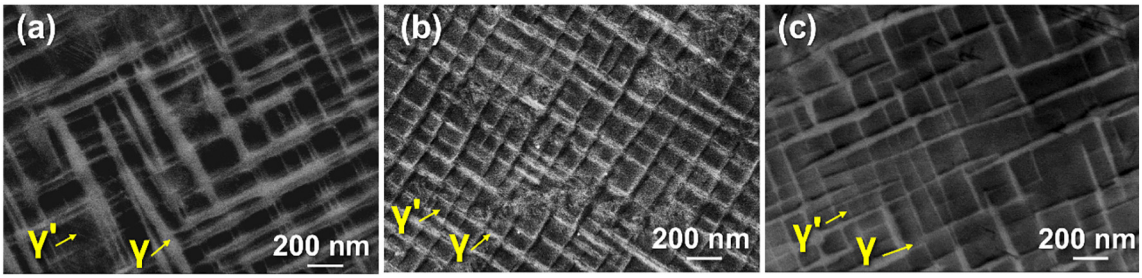

Fig. 1. BSE images of (a) Co-12Ti, (b) Co-12Ti-4Mo, and (c) Co-12Ti-4Cr after aging at 800 °C for 24 h. BSE: Back scattered electrons.

performed from room temperature to 1450 °C at a heating rate of 10 °C/min. To accurately resolve [001] lattice planes in APT analyses, grains with [001] orientation were identified using electron backscatter diffraction (EBSD). Wedge-shaped bars were cut and lifted out from those grains using a dual beam focused-ion-beam (FIB) instrument (Helios NanoLab 600i). The bars were attached to commercial flat-top Si micro tips and subsequently ion-milled into needle-shaped APT specimens according to the procedure described in Ref. [23]. The specimens were cleaned by a final step at a 5 kV acceleration voltage at a current of 41 pA to remove the regions severely damaged by Ga implantation. APT analyses were performed using a CAMECA LEAP™ 5000XS system in laser pulsing mode at a specimen base temperature of 40 K. A laser pulse frequency of 200 kHz and a pulse energy of 40 pJ were applied. Data analysis was performed with the software IVAS™ 3.6.14.

Fig. 1(a)–(c) shows BSE images of the aged Co-12Ti, Co-12Ti-4Mo, and Co-12Ti-4Cr samples. Two-phase γ/γ′ microstructures can be clearly observed for all three alloys. The γ channels and γ′ precipitates show bright and dark contrast, respectively, because of the difference in the average atomic number. [24,25]. The γ′ precipitates in the binary Co-12Ti alloy (Fig. 1(a)) are plate-shaped rather than cubic with an average length of 82 ± 12 nm. Such a precipitate morphology suggests that the γ/γ′ interfaces of the Co-12Ti alloy might be semi-coherent [26]. Using X-ray diffraction, we measured a γ/γ′ lattice misfit value of 1.17% for the Co-12Ti alloys (see Fig. S1 in Supplementary material), which is in good agreement with previous reports [10]. The relatively large lattice misfit favors the development of plate-shaped γ′ over cubic γ′ during aging at 800 °C. Aging at higher temperature for longer time, e.g. at 900 °C for 100 h, results in an irregular morphology, as reported by Zenk et al. [21]. Such a drastic change in γ′ morphology with varying aging conditions suggests that Co_3Ti precipitates are prone to coarsening.

Fig. 1(b) and (c) shows that two-phase γ/γ′ microstructures can also be observed for the aged Co-12Ti-4Mo and Co-12Ti-4Cr alloys, where these two ternary alloys exhibit nearly cubic γ′ precipitates. The measured lattice misfit values of Co-12Ti-4Mo and Co-12Ti-4Cr were 1.01% (Fig. S2) and 0.35% (Fig. S3), respectively, and hence lower than for Co-12Ti. The decrease in lattice misfit upon alloying with Mo and Cr is in agreement with the observed changes in γ′ morphology.

Fig. 2(a)–(c) shows proximity histograms [27] across the γ/γ′ interfaces of Co-12Ti, Co-12Ti-4Mo, and Co-12Ti-4Cr alloys, respectively. The proximity histograms reveal that Co and Cr partition to the γ phase, whereas Ti and Mo partition to the γ′ phase, in agreement with recent observations by Zenk et al. [10]. Individual γ and γ′ phase regions were selected from the APT datasets to determine the phase compositions directly from the corresponding mass spectra. The respective compositions of γ and γ′, elemental partitioning coefficients ($K_i = C_i^{\gamma'}/C_i^{\gamma}$), γ′ volume fractions, and phase transition temperatures are listed in Table 1. In the binary Co-12Ti alloy, Co partitions to γ and Ti to γ′. The Ti concentration in γ′ is 20.2 ± 0.1 at.% and thus deviates from the expected stoichiometry of the Co_3Ti phase. This experimental finding suggests the existence of anti-site defects in γ′, where excess Co atoms occupy Ti-sublattice sites. Such an assumption is in line with studies of single phase Co_3Ti, reported to exist in the range from 20 to 25 at.% Ti

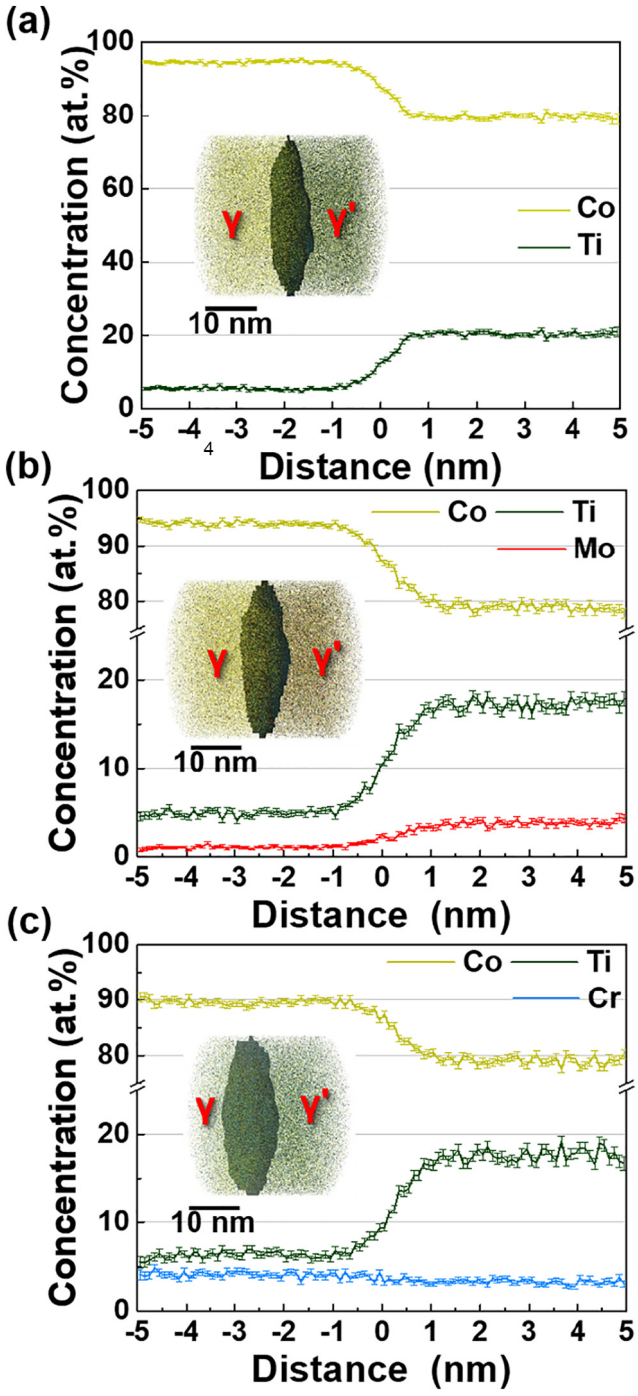

Fig. 2. Proximity histograms across γ/γ′ interfaces of (a) Co-12Ti (12.65 at.% Ti isoconcentration surface is the chosen reference γ/γ′ interface), (b) Co-12Ti-4Mo (10.36 at.% Ti isoconcentration surface) and (c) Co-12Ti-4Cr (10.67 at.% Ti isoconcentration surface) alloys.

Table 1
γ′/γ phase compositions, partitioning coefficients, γ′ volume fractions and phase transition temperatures for Co-12Ti, Co-12Ti-4Mo and Co-12Ti-4Cr alloys.

Alloys		Co-12Ti	+4Mo	+4Cr
γ′/γ concentration (at.%)	Co	79.8/93.6	79.1/93.8	79.6/88.9
	Ti	20.2/6.4	16.4/4.9	17.1/6.6
	Ternary	–	4.5/1.2	3.4/4.5
Partitioning coefficients ($K_x = C_x^{\gamma'}/C_x^{\gamma}$)	Co	0.9	0.8	0.9
	Ti	3.2	3.3	2.6
	Ternary	–	3.7	0.8
γ′ vol. fraction (%)		40.7	65.3	51.8
$T_{\gamma' \text{ solvus}}$ (°C)		1005	1119	1062
$T_{Solidus}$ (°C)		1219	1193	1205
$T_{Liquidus}$ (°C)		1318	1290	1321

due to partial substitution of Ti by Co [28,29]. In Co-12Ti-4Mo, Mo strongly partitions to the γ′ phase, whereas, in Co-12Ti-4Cr, Cr weakly partitions to the γ matrix (compare partitioning coefficients in Table 1).

Using the lever rule, the γ′ volume fractions can be estimated from the phase composition values (for lever rule plot see Fig. S4) [8]. The lever rule can be simply applied to the samples studied herein, since they all exhibit two-phase γ/γ′ microstructures. No other phases can be observed even at grain boundaries (see Fig. S5, Supplementary information). The measured γ′ volume fraction in binary Co-12Ti is ~40.7%, and it increases to 65.3% and 51.8% with the addition of Mo and Cr respectively. The γ′ volume fraction of the Co-12Ti-4Mo alloy is close to the optimum value required for high-temperature creep resistance of γ/γ′-strengthened Ni-based superalloys [30,31]. In addition, the measured γ′ solvus temperature of Co-12Ti-4Mo is 1119 °C and thus substantially higher than the γ′ solvus temperature of binary Co-12Ti (1005 °C) and of Co-9.2Al-9W (990 °C) (Fig. S6, Supplementary information) [2]. However, both solidus and liquidus temperatures of γ′ decrease with Mo addition. The Co-12Ti-4Cr alloy also exhibits an increased γ′ solvus temperature of 1062 °C but this increase is smaller than that of Co-12Ti-4Mo. Overall, we observe an increased thermal stability of γ′ with the addition of Cr and Mo to the Co-12Ti binary.

Fig. 3(a) shows a cumulative histogram of the ion impact positions on the position-sensitive detector of the APT instrument, i.e. field desorption map, acquired from the analysis of a Co-12Ti specimen. We can clearly identify a [001] pole (showing four-fold symmetry) nearly parallel to the tip axis, as expected from the EBSD-guided specimen preparation. Fig. 3(b) presents the corresponding APT reconstruction (yellow green: Co atom, dark green: Ti atom). The γ/γ′ interfaces are highlighted by Ti isoconcentration surfaces encompassing regions of ≥12.65 at.% Ti. A subset of this point cloud across this interface, shown in Fig. 3(c), reveals resolved lattice planes in both γ and γ′ along the [001] direction. Ti atoms occupy every second plane in γ′ as marked by red arrows. Element-specific spatial distribution maps (SDMs) [32] can be calculated along a specific orientation within the reconstructed dataset and they can be used to detect site-occupancy in ordered structures [33]. SDMs were acquired in the γ and γ′ phase along the [001] direction, as shown in Fig. 3(d). Within γ, SDMs for Co and Ti exhibit peaks at an average interspacing of approximately 0.18 nm [23]. It can be concluded that Co and Ti atoms are randomly distributed within this disordered γ phase. In contrast, the SDM for Co in γ′ reveals alternating high and low peaks every 0.18 nm, whereas for Ti, peaks appear at an average distance of 0.36 nm [23,34]. These findings give clear evidence for $L1_2$-type ordering of Co and Ti.

Fig. 4 shows SDMs calculated along the [001] direction in γ′ for both Co-12Ti-4Mo and Co-12Ti-4Cr. Mo shows periodic peaks with an average interspacing of about 0.36 nm identical to Ti (Fig. 4(a)), indicating that Mo occupies the Ti-sublattice sites in γ′ [35]. This observation is consistent with the measured drop in the Ti concentration in γ′ from 20.2% to 16.4% (see Table 1). Furthermore, the solubility of Ti in γ appears to be reduced by the addition of Mo to the binary alloy, as the Ti concentration in aged Co-12Ti-4Mo is 4.9 at.% Ti, as compared to 6.4 at.% Ti in aged Co-12Ti. Overall, Mo increases the partitioning coefficient of Ti (compare values for Co-Ti and Co-Ti-Mo in Table 1). As Ti has a strong tendency to partition to γ′, excess Ti resulting from partial substitution of Ti by Mo in γ′ contributes to the formation of additional γ′. We conclude that strong partitioning of Mo to γ′ and its tendency to occupy the Ti-sublattice within γ′ as well as a reduced Ti solubility in γ are

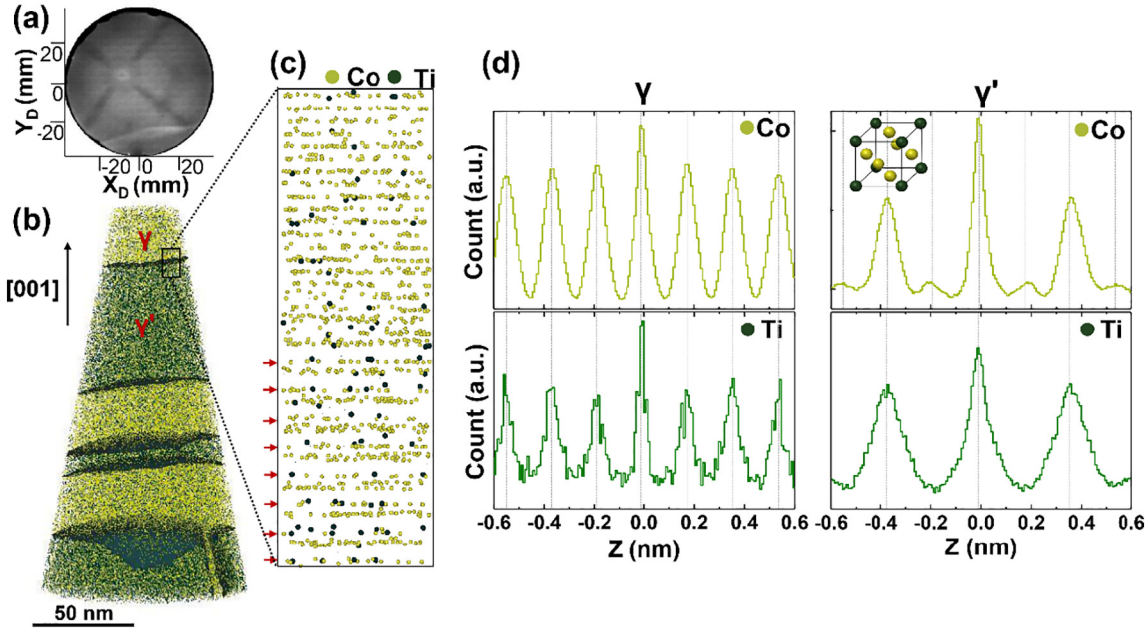

Fig. 3. (a) Field desorption map acquired from an APT analysis of a Co-12Ti sample. (b) APT reconstruction of the tip aligned along the [001] direction. γ/γ′ interfaces are highlighted by 12.65 at.% Ti isoconcentration surfaces. (c) Resolved [001] lattice planes in γ and γ′ phases across the interface. Lattice planes preferentially occupied by Ti atoms are marked with red arrows. (d) Spatial distribution maps (SDMs) of Co and Ti in γ and γ′ phases along the [001] direction. A schematic of the $L1_2$-ordered unit cell (yellow green: Co atom, dark green: Ti atom) was added as an inset to the SDM of Co in γ′. (For interpretation of the references to color in this figure legend, the reader is referred to the web version of this article.)

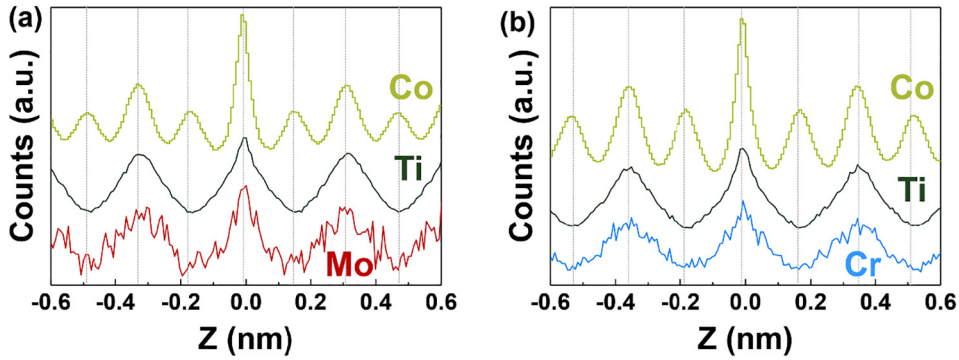

Fig. 4. Elemental SDMs along the [001] direction in γ′ for (a) Co-12Ti-4Mo and (b) Co-12Ti-4Cr along the [001] direction.

the key factors for the observed increase in the γ′ volume fraction upon alloying with Mo.

Fig. 4(b) shows SDMs for Co, Cr and Ti in γ′ for the Co-12Ti-4Cr alloy, which are very similar to the SDMs obtained for the same elements in the Co-12Ti-4Mo alloy. The Ti concentration in γ′ decreases to 17.1% with the addition of Cr. Although Cr preferentially partitions to γ (see Table 1), Cr in γ′ substitutes mostly Ti, thus leading to an increase in γ′ volume fraction, by virtue of the same mechanism as for Mo. However, Cr strongly reduces the partitioning coefficient of Ti. As can be seen in Table 1, the solubility of Ti in γ is little affected by Cr, which leads to a modest increase in γ′ volume fraction for the Co-12Ti-4Cr alloy as compared to the reference Co-12Ti alloy.

In conclusion, our investigation showed that Co-12Ti, Co-12Ti-4Mo and Co-12Ti-4Cr alloys when aged at 800 °C for 24 h exhibit a γ/γ′ microstructure, with both Mo and Cr addition leading to an increase in the γ′ volume fraction and γ′ solvus temperature. Mo strongly partitions to γ′, acting like a typical γ′ stabilizer, which contrasts with Cr partitioning to γ. Elemental SDMs in the γ′ phase give strong evidence that Mo and Cr occupy Ti sites in the $L1_2$-ordered structure, which, in turn, results in an increase in the γ′ volume fraction. The atomic-scale insights gained from our studies can be exploited for designing more advanced γ/γ′-strengthened Co-Ti based superalloys with superior γ′ phase stability and high temperature properties. We also consider the data presented herein as highly relevant for understanding the atomic-scale mechanisms and kinetics of γ′ precipitation in Co-Ti-based systems as a function of alloy composition. These issues will be addressed in a future study.

Acknowledgements

This work was supported by the National Research Foundation of Korea (NRF) [grant number 2016R1A2B4012426]; the U.S. Air Force Office of Scientific Research (AFOSR) [grant number FA2386-16-1-4120]. HI acknowledges financial support of R&E Initiative for Emerging Materials-based Creative Convergence. HI, SKM, BG, DR are grateful to U. Tezins and A. Sturm for their technical support of the atom probe tomography and focused ion beam facilities at the Max-Planck-Institut für Eisenforschung. SKM also acknowledges financial support from the Alexander von Humboldt Foundation.

Appendix A. Supplementary data

Supplementary data to this article can be found online at https://doi.org/10.1016/j.scriptamat.2018.05.041.

References

[1] C.S. Lee, Precipitation-hardening Characteristics of Ternary Cobalt-aluminum-X Alloys, (Ph.D. Thesis) The University of Arizona, Arizona, USA, 1971.
[2] J. Sato, T. Omori, K. Oikawa, I. Ohnuma, R. Kainuma, K. Ishida, Science 312 (2006) 90.
[3] S. Meher, H.Y. Yan, S. Nag, D. Dye, R. Banerjee, Scr. Mater. 67 (2012) 850.
[4] T.M. Pollock, J. Dibbern, M. Tsunekane, J. Zhu, A. Suzuki, JOM 62 (2010) 58.
[5] H. Mughrabi, Acta Mater. 81 (2014) 21.
[6] S. Kobayashi, Y. Tsukamoto, T. Takasugi, H. Chinen, T. Omori, K. Ishida, S. Zaefferer, Intermetallics 17 (2009) 1085.
[7] S. Kobayashi, Y. Tsukamoto, T. Takasugi, Intermetallics 31 (2012) 94.
[8] I. Povstugar, P.P. Choi, S. Neumeier, A. Bauer, C.H. Zenk, M. Göken, D. Raabe, Acta Mater. 78 (2014) 78.
[9] S.K. Makineni, B. Nithin, D. Palanisamy, K. Chattopadhyay, J. Mater. Sci. 51 (2016) 7843.
[10] C.H. Zenk, I. Povstugar, R. Li, F. Rinaldi, S. Neumeier, D. Raabe, M. Göken, Acta Mater. 135 (2017) 244.
[11] I. Povstugar, C.H. Zenk, R. Li, P.-P. Choi, S. Neumeier, O. Dolotko, M. Hoelzel, M. Göken, D. Raabe, Mater. Sci. Technol. 32 (2016) 220.
[12] S.K. Makineni, B. Nithin, K. Chattopadhyay, Scr. Mater. 98 (2015) 36.
[13] S.K. Makineni, B. Nithin, K. Chattopadhyay, Acta Mater. 85 (2015) 85.
[14] S.K. Makineni, A. Samanta, T. Rojhirunsakool, T. Alam, B. Nithin, A.K. Singh, R. Banerjee, K. Chattopadhyay, Acta Mater. 97 (2015) 29.
[15] M. Jiang, G. Saren, S.Y. Yang, H.X. Li, S.M. Hao, Trans. Nonferrous Metals Soc. China 21 (2011) 2391.
[16] J.J. Ruan, X.J. Liu, S.Y. Yang, W.W. Xu, T. Omori, T. Yang, B. Deng, H.X. Jiang, C.P. Wang, R. Kainuma, K. Ishida, Intermetallics 92 (2018) 126.
[17] T. Takasugi, S. Hirakawa, O. Izumi, S. Ono, S. Watanabe, Acta Metall. 35 (1987) 2015.
[18] T. Takasugi, O. Izumi, Acta Metall. 33 (1985) 39.
[19] T. Takasugi, O. Izumi, Acta Metall. 34 (1986) 607.
[20] Y. Liu, T. Takasugi, O. Izumi, H. Suenaga, J. Mater. Sci. 24 (1989) 4458.
[21] C.H. Zenk, S. Neumeier, H.J. Stone, M. Göken, Intermetallics 55 (2014) 28.
[22] T. Takayama, M.Y. Wey, T. Nishizawa, Trans. Jpn. Inst. Metals 22 (1981) 315.
[23] S. Meher, P. Nandwana, T. Rojhirunsakool, J. Tiley, R. Banerjee, Ultramicroscopy 148 (2015) 67.
[24] G.E. Lloyd, Mineral. Mag. 51 (1987) 3.
[25] C.H. Zenk, S. Neumeier, N.M. Engl, S.G. Fries, O. Dolotko, M. Weiser, S. Virtanen, M. Göken, Scr. Mater. 112 (2016) 83.
[26] J.M. Howe, H.I. Aaronson, R. Gronsky, Acta Metall. 33 (1985) 639.
[27] O.C. Hellman, J.A. Vandenbroucke, J. Rüsing, D. Isheim, D.N. Seidman, Microsc. Microanal. 6 (2000) 437.
[28] T. Takasugi, O. Izumi, Acta Metall. 33 (1985) 33.
[29] T. Shinohara, T. Takasugi, H. Yamauchi, T. Kamiyama, H. Yamamoto, O. Izumi, J. Phys. F: Met. Phys. 16 (1986) 1845.
[30] Y. Ro, Y. Koizumi, H. Harada, Mater. Sci. Eng. A 223 (1997) 59.
[31] T. Murakumo, Y. Koizumi, K. Kobayashi, H. Harada, in: K.A. Green, et al., (Eds.), Superalloys, TMS, Warrendale, PA 2004, pp. 155–162.
[32] B.P. Geiser, T.F. Kelly, D.J. Larson, J. Schneir, J.P. Roberts, Microsc. Microanal. 13 (2007) 437.
[33] B. Gault, X.Y. Cui, M.P. Moody, F.D. Geuser, C. Sigli, S.P. Ringer, A. Deschamps, Scr. Mater. 66 (2012) 903.
[34] Q. Yao, H. Xing, J. Sun, Appl. Phys. Lett. 89 (2006) 161906.
[35] S. Meher, R. Banerjee, Intermetallics 49 (2014) 138.